Journal of Nuclear Medicine, published on January 30, 2021 as doi:10.2967/jnumed.120.258384

Synthesis and Preclinical Evaluation of ^{68}Ga-labeled Adnectin, ^{68}Ga-BMS-986192 as a PET Agent for Imaging PD-L1 Expression

Stephanie Robu*[1], Antonia Richter[†1], Dario Gosmann[†2], Christof Seidl[1], David Leung[3], Wendy Hayes[3], Daniel Cohen[3], Paul Morin[3], David J Donnelly[3], Daša Lipovšek[3], Samuel J Bonacorsi[3], Adam Smith[3], Katja Steiger[4,5], Christina Aulehner[2], Angela M Krackhardt[2,5], Wolfgang A Weber[1,5,6]

[1] Technical University of Munich, Department of Nuclear Medicine, Klinikum rechts der Isar, Ismaningerstr. 22, 81675 München, Germany

[2] Technical University of Munich, School of Medicine, Klinikum rechts der Isar, Clinic and Policlinic for Internal Medicine III

[3] Bristol-Myers Squibb Research and Development, Route 206 & Province Line Rd., Princeton, 08543 New Jersey, USA

[4] Technical University of Munich, School of Medicine, Institute of Pathology

[5] German Cancer Consortium (DKTK), partner-site Munich; and German Cancer Research Center (DKFZ) Heidelberg, Germany

[6] TranslaTUM (Zentralinstitut für translationale Krebsforschung der Technischen Universität München), Ismaningerstr. 22, 81675 München, Germany

[†] Contributed equally to this work.

Word Count: 5083 words

* to whom correspondence should be addressed

Stephanie Robu
Department of Nuclear Medicine
Klinikum rechts der Isar
Technical University Munich
Ismaningerstr. 22
81675 München
Germany
Phone: +49 89 4140 6315
Fax: +49 89 4140 4989
stephanie.robu@tum.de

ABSTRACT

Blocking the interaction of the immune checkpoint molecules programmed cell death protein-1 (PD-1) and its ligand, PD-L1, using specific antibodies has been a major breakthrough for immune oncology. Whole-body PD-L1 expression positron emission tomography (PET) imaging may potentially allow for a better prediction of response to PD-1 targeted therapies. Imaging of PD-L1 expression is feasible by PET with the Adnectin protein ^{18}F-BMS-986192. However, radiofluorination of proteins, such as BMS-986192 remains complex and labelling yields are low. The goal of this study was therefore the development and preclinical evaluation of a ^{68}Ga-labeled Adnectin protein (^{68}Ga- BMS-986192) to facilitate clinical trials.

Methods

^{68}Ga-labeling of DOTA-conjugated Adnectin (BXA-206362) was carried out in NaOAc-buffer at pH 5.5 (50°C, 15min). *In vitro* stability in human serum at 37°C was analyzed using Radio-thin layer chromatography (Radio-TLC) and Radio-high performance liquid chromatography (Radio-HPLC). PD-L1 binding assays were performed using the transduced PD-L1 expressing lymphoma cell line U-698-M and wild-type U-698-M cells as negative control. Immunohistochemical staining studies, biodistribution and small animal PET studies of ^{68}Ga-BMS-986192 were carried out using PD-L1-positive and negative U-698-M-bearing NSG mice.

Results

^{68}Ga-BMS-986192 was obtained with quantitative radiochemical yields (RCYs) >97% and with high radiochemical purity (RCP). *In vitro* stability in human serum was ≥ 95% after 4h of incubation. High and specific binding of ^{68}Ga-BMS-986192 to human PD-L1-expressing cancer cells was confirmed, which closely correlates with the respective PD-L1 expression level determined by flow cytometry and IHC staining. *In vivo*, ^{68}Ga-BMS-986192 uptake was high in PD-L1+ tumors (9.0±2.1%ID/g at 1hp.i.) and kidneys (56.9±9.2% ID/g at 1hp.i.) with negligible uptake in other tissues. PD-L1 negative tumors

demonstrated only background uptake of radioactivity (0.6±0.1% ID/g). Co-injection of an excess of unlabelled Adnectin reduced tumor uptake of PD-L1 by more than 80%.

Conclusion

^{68}Ga-BMS-986192 enables easy radiosynthesis and shows excellent *in vitro* and *in vivo* PD-L1 targeting characteristics. The high tumor uptake combined with low background accumulation at early imaging time points demonstrate the feasibility of ^{68}Ga-BMS-986192 for imaging of PD-L1 expression in tumors and is encouraging for further clinical applications of PD-L1 ligands.

Key Words

PD-1/PD-L1 checkpoint inhibitors, PD-L1 PET Imaging, ^{68}Ga-Adnectin, ^{68}Ga-BMS-986192, ^{18}F-BMS-986192

INTRODUCTION

The immune system is in principle capable to recognize and destroy cancer cells even in the presence of larger tumor masses and multiple metastases (*1*). However, cells of the innate and adaptive immune systems are frequently inhibited by molecular pathways that suppress their activation and effector functions and allow tumor cells to escape immune recognition and attack (*2*). One major checkpoint that is exploited by cancer cells to evade the immune system is the programmed death protein-1 (PD-1) pathway. The negative costimulatory receptor PD-1 is expressed on the surface of activated T cells (*3,4*). Its ligand the programmed death protein ligand 1 (PD-L1), a surface protein, is expressed on both antigen-presenting cells and tumor cells of a variety of human cancers (*5-7*). PD-1/PD-L1 interaction induces downregulation of T-cell activation and allows tumor cells to evade immune recognition and elimination (*8*).

Inhibition of the PD-1/PD-L1 interaction by antibodies has been a breakthrough for the treatment of several common malignancies such as melanoma, non-small cell lung cancer, renal cell carcinoma, and urothelial cancer (*9-12*). However, only a subgroup of the patients responds to this immune checkpoint inhibitor treatment and the underlying reasons are not well understood (*13-16*). Several studies demonstrated that response to PD-1/PD-L1-targeted immunotherapy correlates with PD-L1 expression levels on tumor tissue of diverse malignancies as determined by immunohistochemistry (*17*). However, the quantitative analysis of PD-L1 expression in the tumor tissue is challenging due to the heterogeneous and dynamic expression of such immune checkpoint molecules (*18-21*). Prediction of response to PD-1 targeted therapy by immunohistochemistry is therefore limited and in several tumor types patients benefit from PD-1 targeted therapies in the absence of significant PD-L1 expression in the tumor tissue (*17,22-23*).

Imaging of PD-L1 expression can overcome several of the fundamental limitations of PD-L1 immunohistochemistry. First, imaging can provide a three-dimensional measure for overall PD-L1 expression of a tumor, whereas as only a very small fraction of the tumor tissues can be routinely studied by immunohistochemistry. Second, imaging can assess PD-L1 expression at the whole-body level and therefore allows for studies of the heterogeneity of PD-L1 expression across multiple metastases in an individual patient. Third, imaging is non-invasive and can therefore not only provide information on PD-L1 status before start of PD-L1 treatment but as well monitor changes of PD-L1 expression at multiple times during treatment. Thus, PD-L1 imaging enables new approaches for studying PD1/PD-L1 pathophysiology in patients and may potentially allow for a better prediction of response to PD-1-targeted therapies than immunohistochemistry (*24*).

It is feasible to image and quantify PD-L1-expression within the tumor in patients with radiolabeled antibodies (*25,26*). However, antibody-based imaging has several disadvantages such as the long circulatory half-life of antibodies and their slow penetration in the tumor tissue which necessitates imaging several days after injection. This requires the use of long-lived radioisotopes for radiolabelling which cause the radiation exposure of antibody positron-emission tomography (PET) to be several-fold higher than of PET with ^{18}F-FDG.

Adnectins are a family of engineered, target binding proteins with a size of ~ 10 kDa, derived from the 10th type III domain of human fibronectin (*27*). Donnelly *et al.* synthesized and evaluated an ^{18}F-labeled anti-PD-L1 Adnectin (^{18}F-BMS-986192) for PET imaging of the PD-L1 expression *in vivo* (*28*). ^{18}F-BMS-986192 showed high *in vivo* stability and excellent anti-PD-L1 targeting characteristics combined with fast renal clearance of the tracer, resulting in high contrast imaging of PD-L1 positive lesions up to hours p.i. (*28*). A first-in-human study with ^{18}F-BMS-986192 in patients with advanced non-small cell lung carcinoma demonstrated a correlation of ^{18}F-Adnectin tumor uptake with PD-L1 expression confirmed by

immunohistochemistry and response to nivolumab treatment on a lesional basis. The authors illustrated that ^{18}F-BMS-986192 SUV_{peak} was higher for responding lesions than non-responding, indicating a correlation of ^{18}F-BMS-986192 PD-L1 PET signal with PD-L1 expression and tumor-level response. (*29*).

However, the multi-step synthesis of ^{18}F-BMS-986192 with only moderate radiochemical yields is challenging and time-consuming (*28,30*). To facilitate a broader clinical application of anti-PD-L1 PET imaging the development of a corresponding ^{68}Ga-labeled analogue based on the Adnectin scaffold seemed the conclusive next step, due to the commercial availability of FDA approved ^{68}Ga/^{68}Ga-generators, the possibility of large-scale cyclotron production of ^{68}Ga and the fast and robust ^{68}Ga-labeling technique. Herein, we report the synthesis and preclinical evaluation of ^{68}Ga-BMS-986192 in terms of PD-L1-affinity, metabolic stability, micro-PET imaging and *in vivo* biodistribution in PD-L1-positive and negative xenografts to investigate the feasibility of this tracer for *in vivo* imaging of PD-L1 expression in tumors.

MATERIALS AND METHODS

Materials

All reagents were obtained from Sigma Aldrich (Munich, Germany) unless otherwise stated. The DOTA-conjugated anti-hPD-L1 Adnectin (BXA-206362), BXA-206362 was kindly provided by Bristol-Myers-Squibb Pharmaceutical Research Institute (New Jersey, USA), formulated in PBS buffer (0.9 mg/mL, pH 7.4) and tested to be endotoxin-free (1.5 EU/mg). ^{68}Ga was obtained from a ^{68}Ge/^{68}Ga generator (Galliapharm, Eckert & Ziegler AG, Berlin, Germany).

Synthesis of ^{68}Ga-BMS-986192 and Quality Control

The generator was eluted in 1 mL fractions with 0.05 M aq. HCl (4 ml) containing 170 – 250 MBq of $^{68}GaCl_3$. To this eluate 1 M NaOAc (100 µl, pH 5.5) and 200 µg DOTA-Adnectin (222 µL in PBS) were added, resulting in a labeling solution at pH 5.5. The solution was mixed briefly and incubated for 15 min at 50°C. ^{68}Ga-BMS-986192 was purified by gel filtration on a PD-10 column (GE Healthcare, Buckinghamshire, UK). Radiochemical yield and radiochemical purity was analyzed by radio-TLC and radio-HPLC. Radio-TLC was performed using Varian silica impregnated ITLC chromatography paper (Varian Inc., CA, USA) and 0.1 M aq. sodium citrate buffer (pH 5.5) as mobile phase. TLC strips were analyzed on a B-FC-3600 TLC Scanner (Bioscan, Washington, USA). Analytical radio-size exclusion chromatography (radio-SEC) of ^{68}Ga-BMS-986192 was carried out using a bioZen SEC-2 (300 x 4.6 mm) column (Phenomenex LTD, Aschaffenburg, Germany) on a Shimadzu HPLC system (0.1 M phosphate buffer, pH 6.8, flow 0.35 ml/min) equipped with a NaI(TI) scintillation detector (2“ x 2“) and a SPD M20A diode array UV/Vis detector.

In Vitro Stability of ^{68}Ga-BMS-986192 in Human Serum

In vitro stability study was carried out by adding ^{68}Ga-BMS-986192 (app. 18 MBq to freshly prepared human serum (1/8, v/v; Seronorm™ Human, IGZ Instruments AG, Zürich), followed by incubation at 37 °C for up to 4 hours. To investigate the stability of ^{68}Ga-BMS-986192 in human serum, radio-HPLC and radio-TLC were performed at 0, 1, 2, 3, and 4 hours.

Cell Culture

The PD-L1 negative B-cell lymphoma cell line U-698-M was purchased from ATCC (Manassas, VA, USA). Cultures were maintained in RPMI medium supplemented with 10% FBS and penicilline/streptomycine (100IU/ml). Cells were grown at 37 °C in a humidified atmosphere of 5% CO_2. To stably express PD-L1 the

U-698-M cells were retrovirally transduced with a construct containing genes for human PD-L1 and GFP, as previously described (*31*). Quantification of PD-L1 expression on transduced and wild-type U-698-M cells was determined by fluorescence activated cell sorting (FACS) analysis using a anti-human CD274 antibody (Clone MIH1; BD Bioscience, Franklin Lakes, USA) as previously described (*32*).

Assessment of PD-L1 Binding Affinity and Specificity

The binding affinity of ^{68}Ga-BMS-986192 towards human PD-L1 was determined in a competitive binding experiment using stable transduced U-698-M PD-L1 cells with elevated PD-L1 expression. Briefly, a solution containing a mixture of ^{68}Ga-labeled (25 µL) and unlabeled DOTA-conjugated anti-hPD-L1 Adnectin (25 µL, competitor) with increasing concentrations (10^{-10} – 10^{-6} M) was added to the cells (400.000 cells/vial). After 1 h incubation at 37 °C, cells were centrifuged at 600 x g (1,200 rpm, Biofuge 15) for 5 min, the supernatant of each vial was removed and cells were thoroughly washed 2 times with 250 µl PBS. The washing media was combined with the previously removed supernatant, representing the amount of free radioligand. The amount of cell bound activity (cell pellet) as well as the amount of free radioligand was measured in a 2470 Wizard^2 ɤ-counter (PerkinElmer, MA, USA). Due to the high structural similarity of ^{68}Ga-labeled and unlabeled ligand a nearly identical affinity for PD-L1 is assumed, resulting in homologous competitive binding. Specific binding was confirmed using non-transduced U-689-M cells as a negative control.

U-698-M Tumor Model

All animal experiments were conducted according the current animal welfare regulations in Germany (DeutschesTierschutzgesetz, approval (ROB-55.2-2532.Vet_02-15-216)). The transduced U-698-M PD-L1 positive and U-698-M wild-type cell line were detached from the surface of the culture flask using

Trypsin/EDTA (0.05% and 0.02%) in PBS, centrifuged and resuspended in PBS. Approximately 1 x 10^7 cells/200µL of the U-698-M PD-L1 positive cell line were inoculated subcutaneously on the right and U-698-M wild-type cells on the left flank of 6 to 8 weeks old NSG mice (male, Charles River WIGA GmbH, Sulzfeld, Germany). Tumors were grown for 2 to 3 weeks to reach 0.6- 1 cm in diameter.

Small-Animal PET-Imaging

Mice were anesthetized with isoflurane and intravenously injected via tail vein with app. 5-7 MBq (~ 4.5 - 5.5 µg) of ^{68}Ga-BMS-986192. *In vivo* imaging studies were performed using a Siemens Inveon small-animal PET/CT scanner. Static images were recorded at 1 h and 2 h p.i. with an acquisition time of 20 min. For blocking studies, unlabeled BXA-206362 (9 mg/kg) was coinjected with ^{68}Ga-BMS-986192. Dynamic imaging was performed after on-bed injection for 1.5 h under isoflurane anesthesia. Reconstruction of the images was carried out using 3-dimensional ordered-subsets expectation maximum (OSEM3D) algorithm with scanner and attenuation correction. Data analysis was carried out using Inveon Workplace software (Siemens). Regions of interest were drawn around areas with increased uptake in transaxial slices for calculation of the average tracer concentration as percent injected activity per milliliter (% IA/mL).

Ex Vivo Histology and Immunohistochemistry

Tumor tissues were fixed in 10% neutral-buffered formalin solution for at least 48 h, dehydrated under standard conditions (Leica ASP300S, Wetzlar, Germany) and embedded in paraffin. Serial 2 µm-thin sections prepared with a rotary microtome (HM355S, Thermo Fisher Scientific, Waltham, USA) were collected and subjected to histological and immunohistochemical analysis. Hematoxylin-Eosin (HE) staining was performed on deparaffinized sections with Eosin and Mayer's Haemalaun according to a standard protocol.

Immunohistochemistry was performed using a Bond RXm system (Leica, Wetzlar, Germany) with primary antibodies against human PD-L1 (clone 28-8, ab205921, 1:500).

Ex-Vivo Biodistribution

About 5-7 MBq of ^{68}Ga-BMS-986192 (4.5 - 5.5 µg) were injected into the tail vein of the U-698-M-PD-L1^{+} and U-698-M wild-type tumor bearing NSG mice under isoflurane anesthesia. Animals were sacrificed at 1h p.i. (n=4) and 2h p.i. (n=4), the organs of interest were dissected, and the activity in the weighed tissues samples was quantified using a γ-counter.

RESULTS

^{68}Ga-Labeling and In Vitro Stability of ^{68}Ga-BMS-986192 in Human Serum

High labeling efficiencies with quantitative radiochemical yields of > 97 % were obtained after 15 min. After purification moderate specific activities (S_A) of 11-16 GBq/µmol and radiochemical purity > 98% was achieved.

Radio-chromatograms of ^{68}Ga-BMS-986192 at various time points after mixing with human serum revealed monomeric elution profiles with a minimal radioactive impurity of higher molecular weight (8.97 min), which slightly increases up to 5% after 4 h. Radio-TLC analysis revealed moderate transmetallation (5%) for ^{68}Ga-BMS-986192 within 4h (Supplemental Fig. 1).

Characterization of PD-L1 Expression in Transduced U-698-M Cells

Quantification of PD-L1 expression on transduced and wild-type U-698-M cells was determined by FACS analysis. A low PD-L1 expression of approximately 4.000 molecules per cell was observed for wild-type U-

698-M cells (Fig. 1). PD-L1 expression was significantly increased by stable transduction of U-698-M cells, with approximately 155.000 PD-L1 molecules per cell.

Competitive Binding Assay of ^{68}Ga-BMS-986192 to PD-L1

Binding affinity of ^{68}Ga-BMS-986192 to human PD-L1 was determined in competitive radioligand binding experiment using PD-L1 positive and wild-type U-698-M cells. ^{68}Ga-BMS-986192 showed high affinity towards human PD-L1 with an IC_{50} value of 2.0 ± 0.6 nM (Fig. 2A). Specific binding was confirmed using non-transduced U-698-M cells as a negative control (Fig. 2B).

PET/CT Imaging

^{68}Ga-BMS-986192 showed a rapid clearance from the blood pool and from non-target tissues with continuously increasing accumulation in the kidneys over time (Figs. 3A and 3B). ^{68}Ga-BMS-986192 uptake in PD-L1 positive tumor was fast within 4 min p.i. and tracer accumulation in PD-L1 expressing tumor tissue increased within 60 min with high retention over 90 min p.i. (Figs. 3A and 3C). No uptake in the PD-L1 negative U-698-M tumor was observed.

Additional static µPET scans were performed with ^{68}Ga-BMS-986192 in PD-L1 positive and PD-L1 wild-type tumor-bearing NSG mice at 1 h p.i and 2 h p.i. (Fig. 4A). ^{68}Ga-BMS-986192 showed comparable high tumor uptake in PDL-1 positive tumors after 1 h and 2 h p.i.. As shown in Figure 4A, in contrast to the high uptake of ^{68}Ga-BMS-986192 in PD-L1 positive U-698-M tumors, no accumulation was observed in U-698-M wild-type xenografts confirming PD-L1 specific binding of ^{68}Ga-BMS-986192. Additionally, blocking experiments with excess of unlabeled Adnectin (9mg/kg) demonstrated that ^{68}Ga-BMS-986192 uptake is specific and PD-L1 mediated (Fig. 4B).

Ex Vivo FACS Analysis, Histology and Immunohistochemistry

Ex vivo FACS analysis of dissected tumors confirmed the correlation of ^{68}Ga-BMS-986192 uptake with PD-L1 expression levels in tumor tissue (Figs. 5A and 5B). PD-L1 expression levels in transduced U-698-M tumors was highly increased in comparison to non-transduced U-698-M wild-type xenografts, confirming the generation of a stable PD-L1 expressing tumor cell line *in vivo* and PD-L1 mediated uptake of ^{68}Ga-BMS-986192.

Ex vivo histology and immunohistochemistry of the xenograft tissues also revealed high and homogeneous PD-L1 expression in U-698-M PD-L1 positive tumors, while no PD-L1 expression was found in U-698-M wildtype tissues (Fig. 5C). These results confirm the PD-L1 specific uptake of ^{68}Ga-BMS-986192 in µPET imaging *in vivo* and correlate with *ex vivo* flow cytometry analysis.

Biodistribution

The biodistribution data of ^{68}Ga-BMS-986192 in PD-L1 positive-U-698-M and U-698-M wild-type tumor-bearing mice (1h and 2h p.i.) are shown in Figure 6 and Supplemental Table 1. The data reflect the results of µPET/CT imaging. ^{68}Ga-BMS-986192 exhibited predominant renal clearance with only slight uptake in the liver and non-targeted tissues. The significant uptake of ^{68}Ga-BMS-986192 in PD-L1 positive tumor xenografts is highly specific, as accumulation in PD-L1 negative tumors was less than blood pool activity (Supplemental Table 1).

DISCUSSION

This study revealed that the high-affinity PD-L1 binding Adnectin protein BMS-986192, conjugated at the C terminal position with DOTA via maleimide linkage (BXA-206362) can be labeled with ^{68}Ga while retaining high target binding affinity (IC_{50} 2.0 ± 0.6 nM determined in a competitive radioligand binding

assay using PD-L1 positive U-698-M cells). The DOTA- maleimide moiety was conjugated to the cysteine residue engineered into the C-terminus of the Adnectin (*28,30*). The same position within the Adnectin scaffold has been used previously for site-specific conjugation of the ^{18}F-labeled prosthetic group of ^{18}F-BMS-986192 without a significant effect on binding affinity (*28*). ^{19}F-BMS-986192, unmodified and DOTA-conjugated Adnectin displayed picomolar dissociation constants (K_D) against human PD-L1 determined by surface plasmon resonance (data not shown) (*28*). This indicates that conjugation of small molecules to the C-terminus of Adnectin are well tolerated without observable effects on human PD-L1 binding. The ease of tracer preparation, the quantitative radiochemical yields with high radiochemical purity make the synthesis of ^{68}Ga-BMS-986192 fully compatible with the everyday workflow in a clinical radiopharmacy and are well suited for automated radiosynthesis via a module or a kit formulation. Furthermore, the pharmacokinetics of ^{68}Ga-BMS-986192 match very well the 68-minute physical half-life of ^{68}Ga as peak tumor uptake reached a plateau within 60 min post injection. Collectively, these characteristics are highly encouraging for using ^{68}Ga-BMS-986192 to image PD-L1 expression in humans.

Small animal PET and *ex-vivo* biodistribution studies demonstrated excellent targeting of PD-L1 expressing xenografts whereas tracer uptake was low in tumors without PD-L1 expression on immunohistochemistry (Figs. 4 and 5). Specificity of tracer binding was further confirmed by co-injection of an excess of unlabelled BMS-986192 which decreased tumor uptake of ^{68}Ga-BMS-986192 by 80% (Fig. 6). As expected for a 10 kDa protein, ^{68}Ga-BMS-986192 showed fast, renal clearance from the blood. Similar to other small proteins, peptides and peptide-like molecules we observed also significant retention of activity in the kidney at 1 and 2 h post injection. However, the activity concentration was similar to clinically used PET imaging agents such as prostate specific membrane (PSMA) ligands (*33,34*). Therefore, we do not expect renal uptake of ^{68}Ga-BMS-986192 to limit its clinical use. Injection of an excess of unlabelled adnectin significantly decreased renal uptake of ^{68}Ga-BMS-986192. This is unlikely

due to blocking of PD-L1 binding since BMS986192 has only low affinity for murine PD-L1 (*28*). Nevertheless, it indicates that renal uptake of radioactivity is a partially saturable process that could potentially be reduced by injection of proteins or peptides that do not interfere with the binding of ^{68}Ga-BMS-986192 to its target. The activity concentration in the kidneys increased from 1 to 2 hour post injection probably reflecting redistribution of the ligand from other tissues to the blood stream (Fig. 6).

A comparison of the preclinical results obtained for ^{18}F-BMS986192 and ^{68}Ga-BMS-986192 revealed similar specific activities as well as *in vitro*/*in vivo* behaviour of both tracers (*28*). Although comparable protein and activity doses of ^{18}F-BMS986192 and ^{68}Ga-BMS-986192 were administered to mice, a direct comparison of the tumor uptake of both radiolabelled ligands is not feasible as different cell lines were utilized in the two studies, but both tracers showed similar pharmacokinetics with fast renal clearance and similarly low background activity in all other organs. This is encouraging for the clinical translation of ^{68}Ga-BMS-986192 because PET imaging of PD-L1 expression with ^{18}F-BMS-986192 has already been shown to be feasible in human pilot studies (*29,35*).

The following limitation of the study should be noted. ^{68}Ga-BMS-986192 exclusively binds to human PD-L1 with no relevant affinity towards its murine counterpart (data not shown). Tumor-to-normal organ uptake ratios may therefore be lower in humans than in our mouse model. Furthermore, we used a PD-L1 transduced cell line to study the binding of ^{68}Ga-BMS-986192. The advantages of this approach are that the parent cell line can be used as a negative control to assess specificity of ligand binding. Furthermore, the stable expression of PD-L1 improves the reproducibility of these results to ensure to have a tool for measurement PD-L1 expression of cancer cells, as endogenous cancer cell PD-L1 expression is known to vary significantly over time (*36*). However, PD-L1 expression levels by PD-L1 transduced U698-M cells may be higher than in human tumors.

CONCLUSION

The novel PD-L1 imaging agent ^{68}Ga-BMS-986192 shows similar PD-L1 targeting characteristics and pharmacokinetic properties as ^{18}F-BMS-986192 which has already been successfully used to image PD-L1 expression in cancer patients. In contrast to ^{18}F-BMS-986192 which requires a two-step synthesis with low radiochemical yields, radiolabeling of BMS-986192 with ^{68}Ga is a straightforward one-step process which is easy to automate. ^{68}Ga-BMS-986192 therefore has the potential to significantly facilitate preclinical and clinical imaging of PD-L1 expression.

Disclosure

David Leung, Wendy Hayes, Paul Morin, Adam Smith, David Donnelly, Daša Lipovšek, Sam Bonacorsi, Daniel Cohen are employed by Bristol-Myers Squibb Co. ^{18}F-BMS-986192 and ^{68}Ga-BMS-986192 are the subject of patent applications WO2016086021A1, WO2016086036A2, WO2017/210302 and WO2017/210335. No other potential conflict of interest relevant to this article was reported.

ACKNOWLEDGEMENTS

We thank Sybille Reder, Markus Mittelhäuser and Hannes Rolbiesky for small-animal PET imaging and Olga Seelbach and Marion Mielke for HE- and IHC staining. The current study was financially supported by the Deutsche Forschungsgemeinschaft (SFB824; subproject C10, Z1 and Z2).

KEY POINTS

Question: Can Adnectins be efficiently radiolabeled with ^{68}Ga to allow the *in vivo* assessment and quantification of PD-L1 expression levels on tumor tissue with PET?

Pertinent Findings: The expansion of the Adnectin based concept for PD-L1 expression PET imaging to the requirements of ^{68}Ga-chemistry enables fast and efficient radiolabeling. ^{68}Ga-BMS-986192 showed comparable *in vitro* and *in vivo* PD-L1-targeting characteristics to its counterpart ^{18}F-BMS986192. Both tracers showed favourable pharmacokinetics with fast renal clearance and similarly low background activity in non-targeted tissues.

Implications for Patient Care: The preclinical results are encouraging for the clinical translation of ^{68}Ga-BMS-986192 because PET imaging of PD-L1 expression with ^{18}F-BMS-986192 has already been shown to be feasible in human pilot studies.

REFERENCES

1. Gonzalez H, Hagerling C, Werb Z. Roles of the immune system in cancer: from tumor initiation to metastatic progression. *Genes Dev*. 2018;32:1267-1284.
2. Topalian SL, Drake CG, Pardoll DM. Immune checkpoint blockade: a common denominator approach to cancer therapy. *Cancer Cell*. 2015;27:450-461.
3. Riella LV, Paterson AM, Sharpe AH, Chandraker A. Role of the PD-1 pathway in the immune response. *Am J Transplant*. 2012;12:2575-2587.
4. Keir ME, Butte MJ, Freeman GJ, Sharpe AH. PD-1 and its ligands in tolerance and immunity. *Annu Rev Immunol*. 2008;26:677-704.
5. Konishi J, Yamazaki K, Azuma M, Kinoshita I, Dosaka-Akita H, Nishimura M. B7-H1 expression on non-small cell lung cancer cells and its relationship with tumor-infiltrating lymphocytes and their PD-1 expression. *Clin Cancer Res*. 2004;10:5094-5100.
6. Thompson RH, Gillett MD, Cheville JC, et al. Costimulatory B7-H1 in renal cell carcinoma patients: Indicator of tumor aggressiveness and potential therapeutic target. *ProcNatlAcadSciUSA*. 2004;101:17174-17179.
7. Hino R, Kabashima K, Kato Y, et al. Tumor cell expression of programmed cell death-1 ligand 1 is a prognostic factor for malignant melanoma. *Cancer*. 2010;116:1757-1766.
8. Freeman GJ, Long AJ, Iwai Y, et al. Engagement of the PD-1 immunoinhibitory receptor by a novel B7 family member leads to negative regulation of lymphocyte activation. *JExpMed*. 2000;192:1027-1034.
9. Herbst RS, Baas P, Kim DW, et al. Pembrolizumab versus docetaxel for previously treated, PD-L1-positive, advanced non-small-cell lung cancer: a randomised controlled trial. *Lancet*. 2016;387:1540-1550.

10. Weinstock M, McDermott D. Targeting PD-1/PD-L1 in the treatment of metastatic renal cell carcinoma. *TherAdvUrol*. 2015;7:365-377.

11. Simeone E, Ascierto PA. Anti-PD-1 and PD-L1 antibodies in metastatic melanoma. *MelanomaManag*. 2017;4:175-178.

12. Stenehjem DD, Tran D, Nkrumah MA, Gupta S. PD1/PDL1 inhibitors for the treatment of advanced urothelial bladder cancer. *OncoTargetsTher*. 2018;11:5973-5989.

13. Alsaab HO, Sau S, Alzhrani R, et al. PD-1 and PD-L1 checkpoint signaling inhibition for cancer immunotherapy: Mechanism, combinations, and clinical outcome. *FrontPharmacol*. 2017;8:561.

14. Chen L, Han X. Anti-PD-1/PD-L1 therapy of human cancer: past, present, and future. *JClinInvest*. 2015;125:3384-3391.

15. Cottrell TR, Taube JM. PD-L1 and emerging biomarkers in immune checkpoint blockade *TherapyCancer J*. 2018;24:41-46.

16. Zou W, Wolchok JD, Chen L. PD-L1 (B7-H1) and PD-1 pathway blockade for cancer therapy: Mechanisms, response biomarkers, and combinations. *Sci TranslMed*. 2016;8:328rv4.

17. Chakravarti N, Prieto VG. Predictive factors of activity of anti-programmed death-1/programmed death ligand-1 drugs: immunohistochemistry analysis. *TransLungCancerRes.* 2015;4:743-751.

18. Kloten V, Lampignano R, Krahn T, Schlange T. Circulating tumor cell PD-L1 expression as biomarker for therapeutic efficacy of immune checkpoint inhibition in NSCLC. *Cells*. 2019;8:809.

19. Yue C, Jiang Y, Li P, et al. Dynamic change of PD-L1 expression on circulating tumor cells in advanced solid tumor patients undergoing PD-1 blockade therapy. *Oncoimmunology*. 2018;7:e1438111.

20. Madore J, Vilain RE, Menzies AM, et al. PD-L1 expression in melanoma shows marked heterogeneity within and between patients: implications for anti-PD-1/PD-L 1 clinical trials. *Pigmentcel melanomaRes*. 2015;28:245-253.

21. Niemeijer A, Leung D, Huisman M, et al. Whole body PD-1 and PD-L1 positron emission tomography in patients with non-small-cell lung cancer. *Naturecommun*. 2018;9:1-5.

22. Ribas A, Hu-Lieskovan S. What does PD-L1 positive or negative mean?. *JExpMed*. 2016;213:2835-2840.

23. Abdel-Rahman O. Correlation between PD-L1 expression and outcome of NSCLC patients treated with anti-PD-1/PD-L1 agents: a meta-analysis. *CritRevOncolHematol.* 2016;101:75-85.

24. Broos K, Lecocq Q, Raes G, Devoogdt N, Keyaerts M, Breckpot K. Noninvasive imaging of the PD-1:PD-L1 immune checkpoint: Embracing nuclear medicine for the benefit of personalized immunotherapy. *Theranostics*. 2018;8:3559-3570.

25. Heskamp S, Hobo W, Molkenboer-Kuenen JD, et al. Noninvasive imaging of tumor PD-L1 expression using radiolabeled anti-PD-L1 antibodies. *CancerRes*. 2015;75:2928-2936.

26. Truillet C, Oh HLJ, Yeo SP, et al. Imaging PD-L1 expression with immunoPET. *BioconjugChem.* 2018;29:96-103.

27. Lipovšek D. Adnectins: engineered target-binding protein therapeutics. *ProteinEngDesSel*. 2011;24:3-9.

28. Donnelly DJ, Smith RA, Morin P, et al. Synthesis and biological evaluation of a novel 18F-labeled adnectin as a PET radioligand for imaging PD-L1 expression. *JNuclMed*. 2018;59:529-535.

29. Niemeijer AN, Leung D, Huisman MC, et al. Whole body PD-1 and PD-L1 positron emission tomography in patients with non-small-cell lung cancer. *NatCommun*. 2018;9:4664.

30. Morin PE, Donnelly D, Lipovsek D, et al. Bristol-Myers Squibb Company, USA. assignee. Novel PD-L1-binding polypeptides for imaging. US patent , WO2016086021A1, 2016.

31. Audehm S, Glaser M, Pecoraro M, et al. Key features relevant to select antigens and TCR from the MHC-mismatched repertoire to treat cancer. *FrontImmunol*. 2019;10:1485.

32. Mayer KE, Mall S, Yusufi N, et al. T-cell functionality testing is highly relevant to developing novel immuno-tracers monitoring T cells in the context of immunotherapies and revealed CD7 as an attractive target. *Theranostics*. 2018;8:6070-6087.

33. Weineisen M, Schottelius M, Simecek J, et al. 68Ga-and 177Lu-labeled PSMA I&T: optimization of a PSMA-targeted theranostic concept and first proof-of-concept human studies. *J Nucl Med.* 2015;56: 1169-1176.

34. Robu S, Schmidt A, Eiber M, et al. Synthesis and preclinical evaluation of novel 18 F-labeled Glu-urea-Glu-based PSMA inhibitors for prostate cancer imaging: a comparison with 18 F-DCFPyl and 18 F-PSMA-1007. *EJNMMIRes.* 2018;8:30.

35. Huisman M, Niemeijer AL, Windhorst B, et al. Quantification of PD-L1 expression with [18F]BMS-986192 PET/CT in patients with advanced stage non-small-cell lung cancer. *JNuclMed*. 2020;61:1455-1460.

36. Yue C, Jiang Y, Li P, et al. Dynamic change of PD-L1 expression on circulating tumor cells in advanced solid tumor patients undergoing PD-1 blockade therapy. *Oncoimmunology*. 2018;7:e1438111.

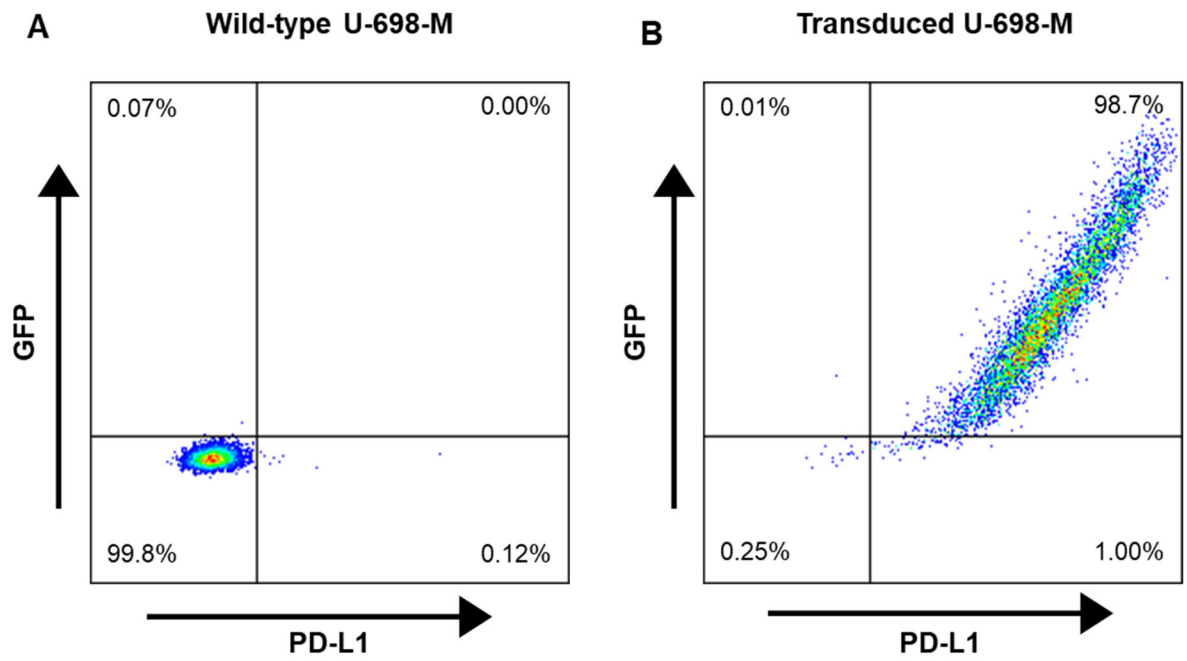

Figure 1 **Generation of a stable PD-L1 expressing U-698-M cell line.** Expression of GFP and PD-L1 of (**A**) U-698-M wild-type cells and (**B**) U-698-M cells transduced by the retroviral vector MP71 containing PD-L1 and GFP separated by a P2A element. Representative dot-plots of U-698-M wild-type and PD-L1 positive U-698-M cells are shown.

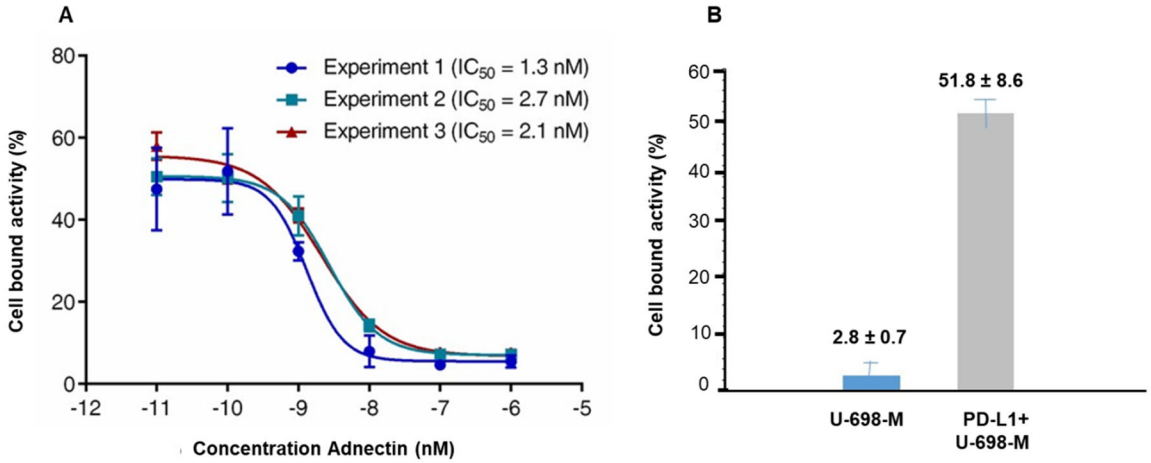

Figure 2 **Binding affinity and specificity of ^{68}Ga-BMS-986192 towards PD-L1 determined in competitive radioligand binding assays.** (**A**) Cell bound activity of ^{68}Ga-BMS-986192 in the presence of increasing concentrations of cold ligand (BXA-206362). (**B**) Cell bound activity of ^{68}Ga-BMS-986192 in the presence of cold ligand (0.1 nM) on PD-L1 positive (U-698-M-PDL1^{+}) and negative U-698-M cells.

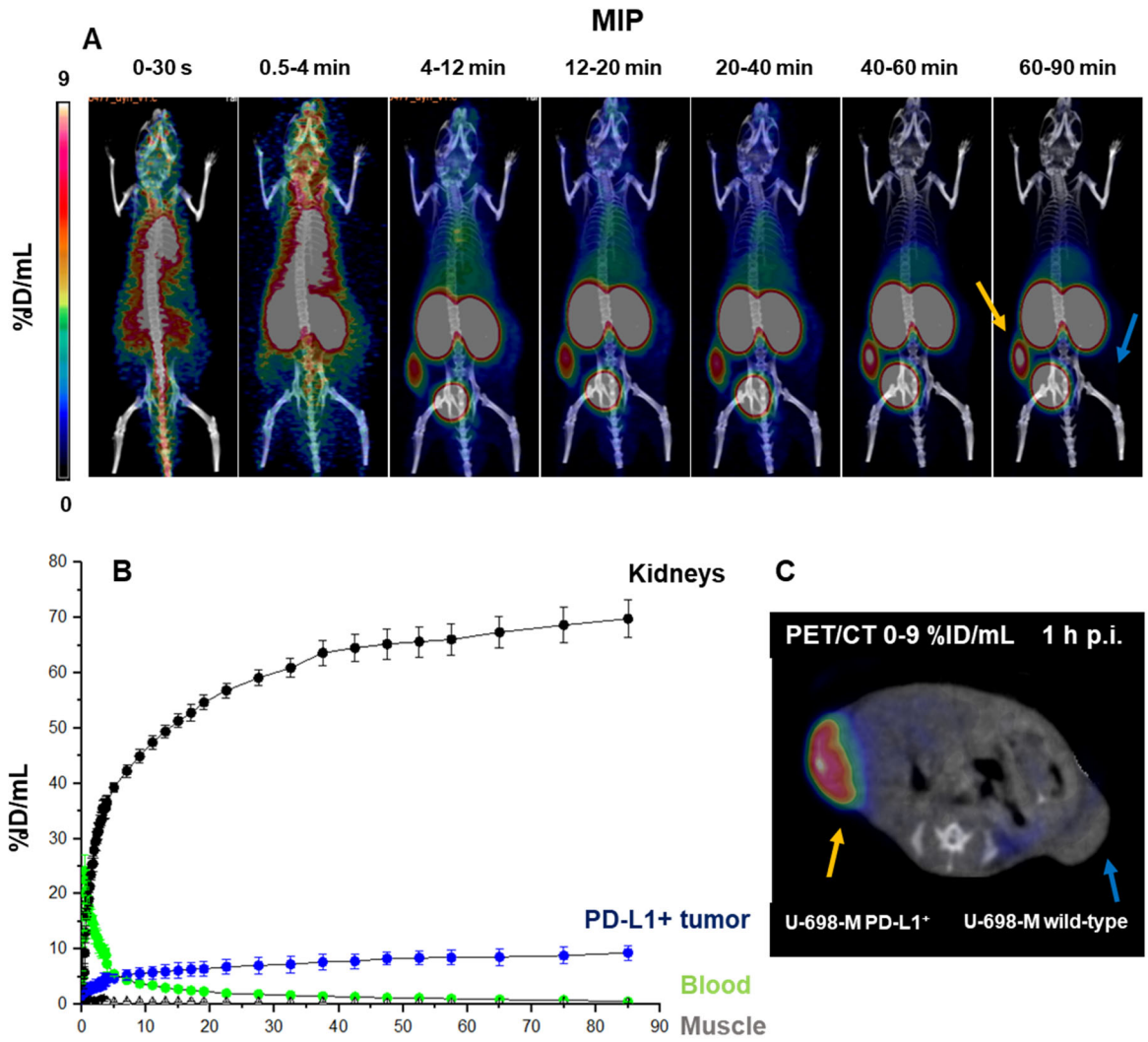

Figure 3 **Dynamic PET imaging in anesthetized mice. A.** Maximum intensity projections (MIP) of a dynamic µPET scan. Summation images of different time-frames (0-9 %ID/mL) of ^{68}Ga-BMS-986192 in PD-L1 positive U-698-M and U-698-M wild-type xenograft bearing mice over an acquisition time of 90 min. **B.** Time-activity curves in %ID/mL for blood pool (heart), kidneys, muscle, and PD-L1 positive tumor derived from dynamic µPET/CT data. **C.** Axial Slice of a ^{68}Ga-BMS-986192 PET/CT scan (1 h p.i.) in a PD-L1 positive U-698-M (yellow arrow) and U-698-M wild-type (blue arrow) xenograft bearing NSG mouse (0-9 %ID/mL).

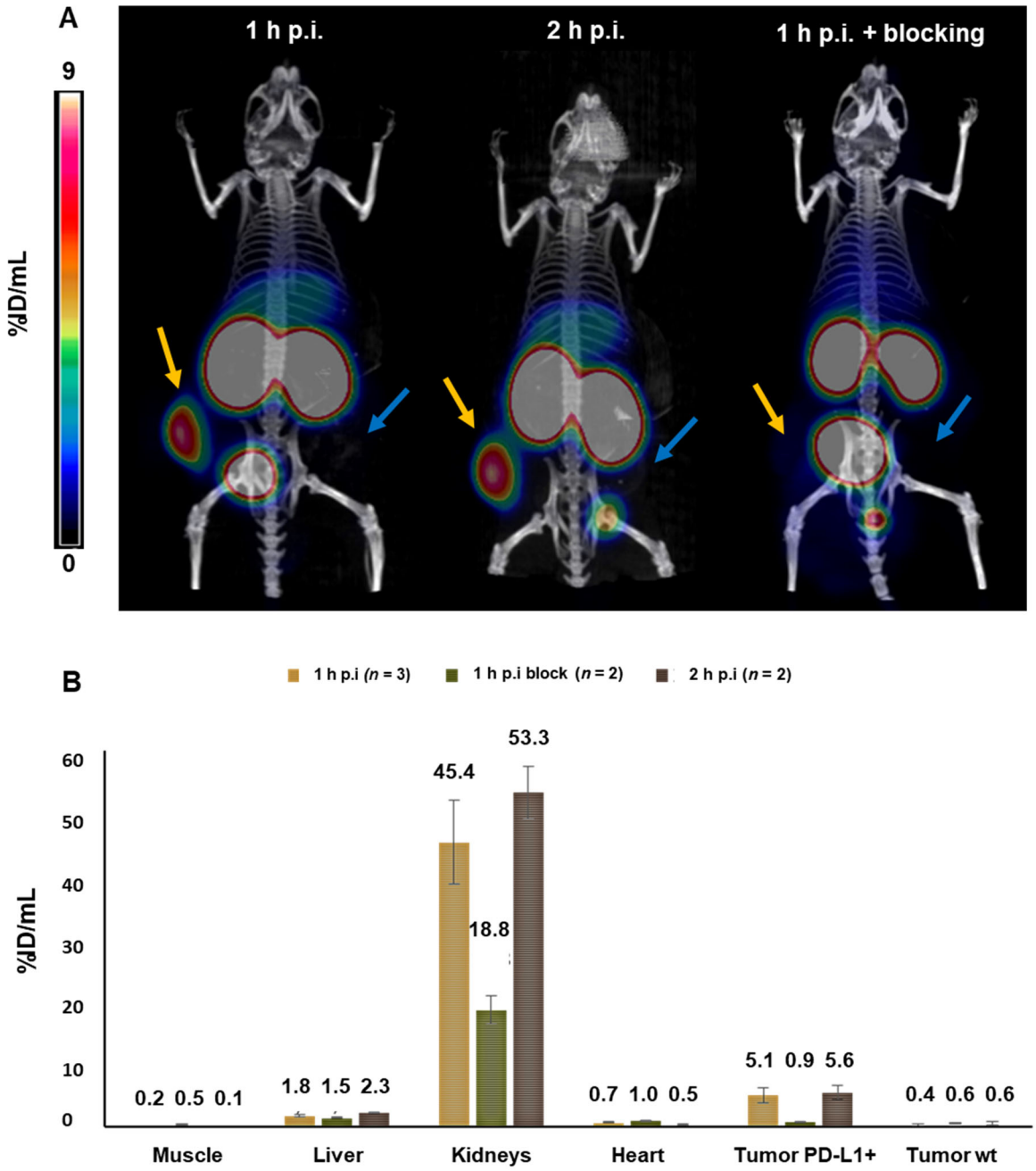

Figure 4 **Static PET imaging examples and quantitative analysis. A.** Maximum intensity projections (MIP) of static µPET scans of ^{68}Ga-BMS-986192 (5-6 MBq, 4.5 - 5.5 µg) 1 h p.i. and 2h p.i. in PD-L1 positive U-698-M (yellow arrows) and U-698-M wild-type (blue arrows) xenograft bearing NSG mice (0% - 9% ID/mL). Mouse 3: Coinjection of ^{68}Ga-BMS-986192 + Blocking with 9 mg/kg unlabeled Adnectin. **B.** ROI Quantification of the static PET scans (%IA/mL $_{mean}$).

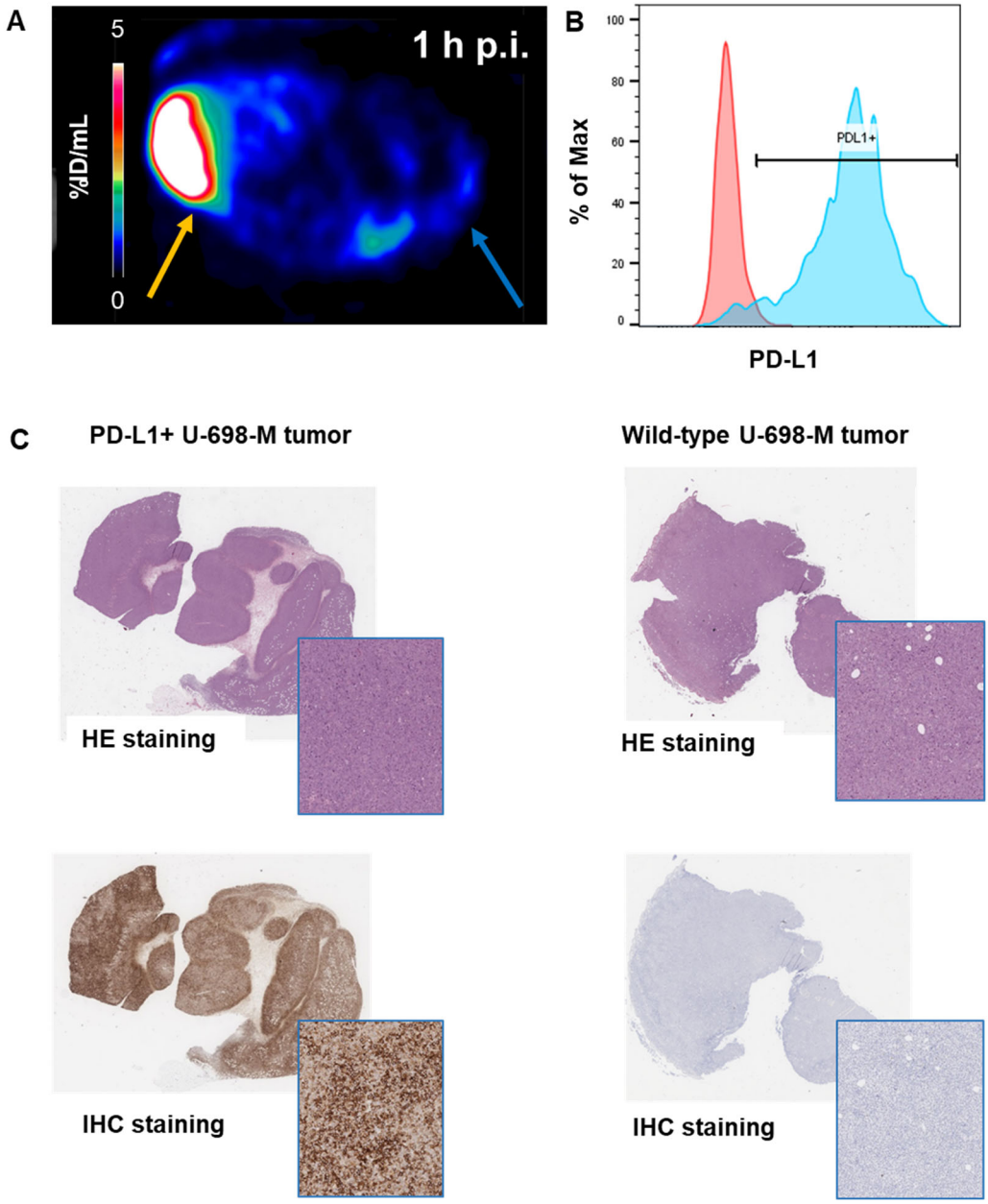

Figure 5 **Comparison of PET, Immunohistochemistry and FACS analysis of tumor xenografts. A.** Axial Slice of a ^{68}Ga-BMS-986192 PET Scan (1 h p.i.) in a PD-L1 positive U-698-M (yellow arrow) and U-698-M wild-type (blue arrow) xenograft bearing NSG mouse (0-5 %ID/ML). **B.** *Ex vivo* FACS analysis of PD-L1 expression on wild-type (red) and PD-L1 transduced (blue) U-698-M tumor cells. **C.** *Ex vivo* HE and anti-PD-L1 immunohistochemistry (IHC) staining of PD-L1 positive and wild-type U-698-M xenograft tissues.

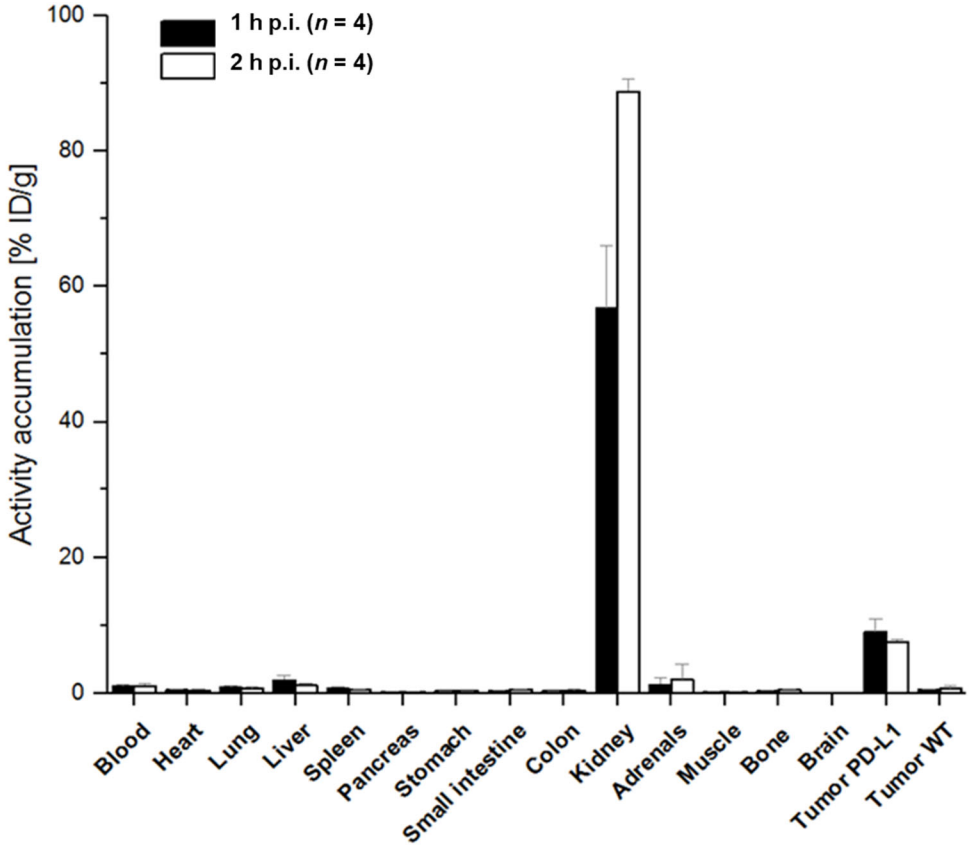

Figure 6 **Biodistribution data of ^{68}Ga-BMS-986192 in PD-L1 positive U-698-M and U-698-M wild-type xenograft bearing mice.** Data are expressed as %ID/g (mean±SD).

Graphical Abstract

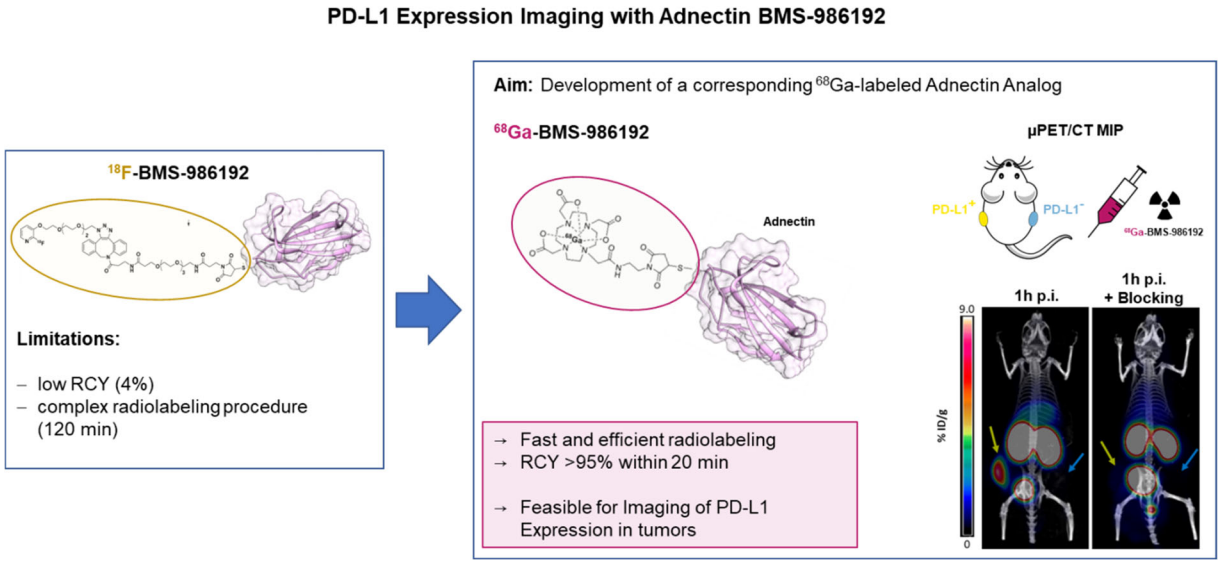

SUPPLEMENTAL DATA

In Vitro Stability of ^{68}Ga-BMS-986192

In vitro stability of ^{68}Ga-BMS-986192 in human serum at 37 °C was determined by Radio-TLC and Radio-HPLC up to 4 h (Supplemental Fig 1).

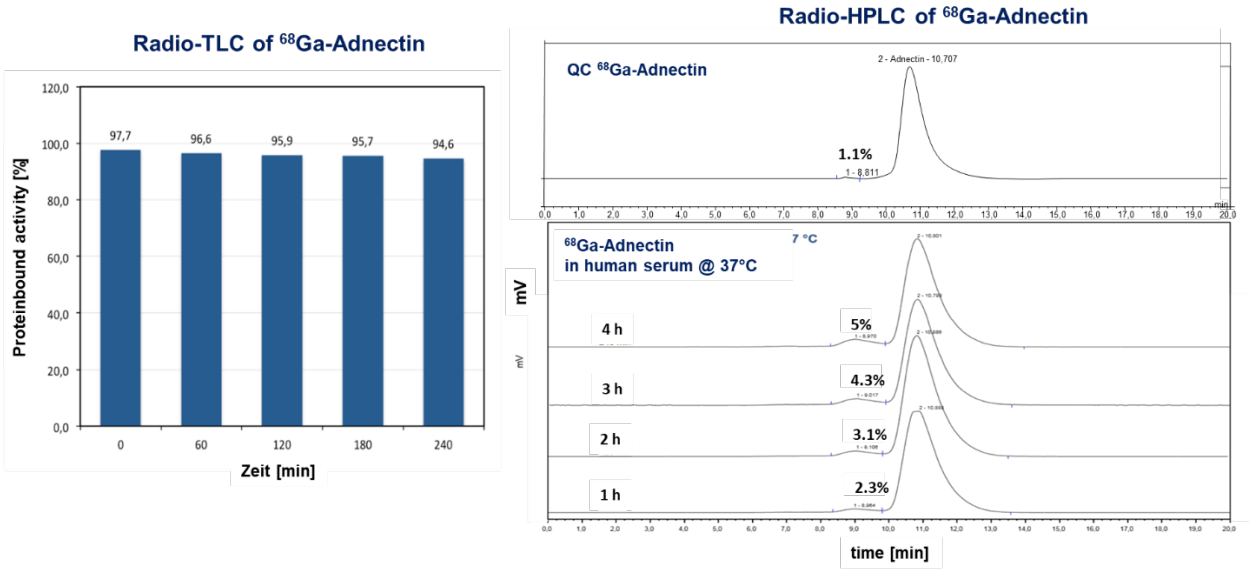

Supplemental Figure 1 | *In vitro* serum stability of ^{68}Ga-Adnectin up to 4 h determined by Radio-TLC and Radio-HPLC.

Ex-Vivo Biodistribution of ^{68}Ga-BMS-986192

Supplemental Table 1 Biodistribution of ^{68}Ga-BMS-986192 in PD-L1 positive U-698-M and U-698-M wild-type bearing NSG mice at 1h and 2h p.i.. Data are given in %ID/g are means ± SD (n=4 animals per group and time point).

Organ	1 h p.i [% ID/g]	2 h p.i. [% ID/g]
Blood	1.0 ± 0.3	1.1 ± 0.3
Heart	0.5 ± 0.1	0.4 ± 0.1
Lung	0.8 ± 0.2	0.7 ± 0.2
Liver	1.9 ± 0.7	1.2 ± 0.2
Spleen	0.7 ± 0.2	0.5 ± 0.2
Pancreas	0.2 ± 0.1	0.2 ± 0.04
Stomach	0.3 ± 0.04	0.3 ± 0.1
Small intestine	0.3 ± 0.1	0.5 ± 0.1
Colon	0.3 ± 0.03	0.4 ± 0.2
Kidney	56.9 ± 9.2	88.9 ± 1.8
Adrenals	1.2 ± 1.0	2.0 ± 2.2
Muscle	0.2 ± 0.1	0.2 ± 0.1
Bone	0.3 ± 0.1	0.5 ± 0.1
Brain	0.04 ± 0.01	0.1 ± 0.04
Tumor PD-L1+	**9.0 ± 2.1**	**7.6 ± 0.4**
Tumor wild-type	**0.6 ± 0.1**	**0.7 ± 0.4**